



Modeling analysis of  
the seasonal  
characteristics of  
haze formation

X. Han et al.

This discussion paper is/has been under review for the journal Atmospheric Chemistry and Physics (ACP). Please refer to the corresponding final paper in ACP if available.

# Modeling analysis of the seasonal characteristics of haze formation in Beijing

X. Han<sup>1</sup>, M. Zhang<sup>1</sup>, J. Gao<sup>2</sup>, S. Wang<sup>2</sup>, and F. Chai<sup>2</sup>

<sup>1</sup>State Key Laboratory of Atmospheric Boundary Layer Physics and Atmospheric Chemistry, Institute of Atmospheric Physics, Chinese Academy of Sciences, HuaYanBeiLi 40# Chaoyang District, Beijing 100029, China

<sup>2</sup>Chinese Research Academy of Environmental Sciences, Beijing 100012, China

Received: 14 October 2013 – Accepted: 13 November 2013 – Published: 21 November 2013

Correspondence to: M. Zhang (mgzhang@mail.iap.ac.cn)

Published by Copernicus Publications on behalf of the European Geosciences Union.

Title Page

Abstract

Introduction

Conclusions

References

Tables

Figures



Back

Close

Full Screen / Esc

Printer-friendly Version

Interactive Discussion



## Abstract

The air quality modeling system RAMS-CMAQ coupled with an aerosol optical property scheme was applied to simulate the meteorological field, major aerosol components (sulfate, nitrate, ammonium, black carbon, organic carbon, dust, and sea salt), and surface visibility over the North China Plain (NCP) in 2011. The modeled results in February and July 2011 were selected and analyzed to obtain an in-depth understanding of the haze formation mechanism in Beijing in different seasons. The evaluations suggested that the modeling system provided reliable simulation results of meteorological factors (temperature, relative humidity, and wind field), visibility, mass concentrations of gaseous pollutants ( $\text{NO}_2$  and  $\text{O}_3$ ), and major aerosol components in  $\text{PM}_{2.5}$  by compared with various observation data at several measurement stations over NCP. The simulation results showed that the visibility below 10 km covered most regions of NCP and dropped below 5 km over the urban areas of Beijing, Tianjin, and Shijiazhuang during the pollution episodes in February and July. The heavy particulate pollutants were concentrated in the same areas as well. The heavy loading of  $\text{PM}_{2.5}$  which could reach  $300 \mu\text{g m}^{-3}$  in Beijing should be the main reason of haze occurrence in February, and the visibility generally decreased to 3–5 km when the mass concentration of  $\text{PM}_{2.5}$  exceeded  $200 \mu\text{g m}^{-3}$ . However, similar values of visibility also appeared in July when the mass concentration of  $\text{PM}_{2.5}$  was merely in the range of  $120 \mu\text{g m}^{-3}$  to  $200 \mu\text{g m}^{-3}$ . Analysis presented that nitrate, sulfate, and ammonium were the three major aerosol components in Beijing and their total mass burden was even higher in July than that in February. Thus, the significantly higher relative humidity and larger mass proportion of soluble aerosol components resulted in more haze days in July. Sensitivity test shows that the mass concentration threshold of  $\text{PM}_{2.5}$  to cause haze occurrence was about  $80 \mu\text{g m}^{-3}$  when the relative humidity was 70 % in Beijing. The change of aerosol size distribution can significantly influence the threshold of haze occurrence in Beijing, particularly for particles of smaller size.

### Modeling analysis of the seasonal characteristics of haze formation

X. Han et al.

Title Page

Abstract

Introduction

Conclusions

References

Tables

Figures

⏪

⏩

◀

▶

Back

Close

Full Screen / Esc

Printer-friendly Version

Interactive Discussion



## 1 Introduction

The emissions of air pollutants have recently increased significantly because of the economic growth, rapid population expansion, and urbanization in the North China Plain (NCP). Beijing, which is the capital of China, has a population of over 20 million and is the political, economic, and cultural center of China. This megacity is located at the northern tip of NCP and surrounded by high mountains in its northern and western boundaries. Beijing has suffered from air quality deterioration in the past decade because of strong local emissions (Sun et al., 2006) and long-range transport from the surrounding urban areas (Zhang et al., 2012) located in the east and south of NCP; such areas include Tianjin, Shijiazhuang, and a number of cities where the economic development is most active in Hebei Province. The air pollution in Beijing is easily aggravated by its special geographic position when stable weather appears or the south wind dominates. Although the SO<sub>2</sub> emission in Beijing in the last five years has been decreased by various measures prescribed by the current legislation on emission controls (Lu et al., 2010; Zhang et al., 2006), the mass burden of particulate pollutants remains at a high level (Hao et al., 2013; Zhang et al., 2013), causing serious environmental issues and associated health effects.

Atmospheric haze is caused by the visibility deterioration (lower than 10 km, Wu et al., 2007) through light extinction by aerosol particles. As a result of the high level of aerosol loadings, widespread haze cloud caused by serious air pollution occurred more frequently over this region in the past decade (Ma et al., 2010; Tao et al., 2012; Wang et al., 2013; Zhao, et al., 2011). A number of studies have investigated the long-term variation features of haze days in Beijing and NCP. Quan et al. (2011) collected monitoring data and summarized the haze day occurrence trend over NCP for the past 56 yr. The said researchers also analyzed the effect of high aerosol loadings on haze formations by conducting a field measurement and found the important role of the hygroscopic growth of aerosols during the haze period. Yu et al. (2010) analyzed the aerosol optical properties during haze days in the past seven years and compared

### Modeling analysis of the seasonal characteristics of haze formation

X. Han et al.

Title Page

Abstract

Introduction

Conclusions

References

Tables

Figures



Back

Close

Full Screen / Esc

Printer-friendly Version

Interactive Discussion



the features of single-scattering albedo and asymmetry factor during haze days with those during dust days in Beijing. This study also found that fine-mode particles were dominant in aerosol size distribution during haze days.

Numerous studies have used multiple methods to investigate the chemical and physical properties of aerosols during haze occurrences in Beijing in different seasons. Li et al. (2013) identified the aerosol size distribution and chemical composition from ground-based remote sensing measurements during haze days in winter. Li et al. (2010) detected the aerosol components by using transmission electron microscopy with energy-dispersive X-ray spectrometry during a haze episode in summer and determined the influence of carbonaceous aerosols. Liu et al. (2012) and Zhao et al. (2013) conducted intensive field experiments to identify the aerosol components of fine particles and discussed the constituent features of PM<sub>2.5</sub> during the haze periods in autumn and winter, respectively. Wang et al. (2006) compared the characteristics of aerosol components during dust, haze, and clean days. These previous works have provided abundant information on the physical and chemical properties of aerosols during haze days. However, the complex mechanism of haze formation over Beijing and its surrounding regions requires further study. Various influencing factors, including meteorological field, key aerosol components, and microphysical properties, should be comprehensively considered in investigating the relationship between aerosols and surface visibility. Moreover, the seasonal similarities and differences of the haze formation mechanism in Beijing remain unclear because most of these studies were generally focused on the pollution periods in the same season.

In the present study, an air quality modeling system called Regional Atmospheric Modeling System–Community Multi-scale Air Quality (RAMS–CMAQ) coupled with aerosol optical property scheme is applied to simulate the meteorological field, the mass burden of major aerosol components (sulfate, nitrate, ammonium, black carbon (BC), organic carbon (OC), dust, and sea salt), and the surface visibility over NCP in 2011. The simulation results in February and July 2011 are selected and analyzed. This study aims to discuss the contributions of various influencing factors to visibility

## Modeling analysis of the seasonal characteristics of haze formation

X. Han et al.

Title Page

Abstract

Introduction

Conclusions

References

Tables

Figures

⏪

⏩

◀

▶

Back

Close

Full Screen / Esc

Printer-friendly Version

Interactive Discussion



deterioration and to compare the differences of the haze formation mechanisms during winter and summer.

## 2 Methodology

The air quality modeling system RAMS–CMAQ was applied to concurrently simulate the atmospheric and land processes that affect the transport, transformation, and deposition of aerosols and their precursors. The major component of this modeling system is CMAQ (version 4.7), which was developed by the US Environmental Protection Agency for assessing the effect of multiple pollutants, including tropospheric ozone and other oxidants, aerosols, and acid deposition (Byun and Schere, 2006; Eder and Yu, 2006; Eder et al., 2009; Mathur et al., 2008). The gas-phase chemistry mechanism was updated to the expanded version CB05 (Sarwar et al., 2008). The thermodynamic equilibrium between inorganic aerosol species and gas-phase concentrations was treated by ISORROPIA (Nenes et al., 1999). Regional Particulate Model (Binkowski and Shankar, 1995) was used to describe the processes of aerosol dynamics in CMAQ; such processes include new particle production, coagulation, and condensation (Bhave et al., 2004; Yu et al., 2013). The aerosol particles in the modeling system were divided into three modes, namely, Aitken, accumulation, and coarse modes (dust and sea salt). All modes were assumed to follow the log normal distribution. The aerosol components, the geometric standard deviation, and the geometric mean radius of each mode are listed in Table 1. The numerical prediction model RAMS was coupled with CMAQ in the offline method to provide CMAQ with a meteorological field. A general description of RAMS and its capabilities have been provided by Cotton et al. (2003). RAMS can efficiently describe the boundary layer and the underlying surface effect, which is important for capturing air pollutants and haze occurrence. The background meteorological fields and sea surface temperature were obtained from the European Center for Medium-Range Weather Forecasts reanalysis datasets ( $1^\circ \times 1^\circ$  spatial resolution) and

### Modeling analysis of the seasonal characteristics of haze formation

X. Han et al.

Title Page

Abstract

Introduction

Conclusions

References

Tables

Figures

⏪

⏩

◀

▶

Back

Close

Full Screen / Esc

Printer-friendly Version

Interactive Discussion





## Modeling analysis of the seasonal characteristics of haze formation

X. Han et al.

Title Page

Abstract

Introduction

Conclusions

References

Tables

Figures

◀

▶

◀

▶

Back

Close

Full Screen / Esc

Printer-friendly Version

Interactive Discussion



For the simulation over NCP, a coarse domain that covers most of East Asia with a horizontal grid distance of 64 km and a total area of 6654 km × 5440 km with a two-way nested inner domain was established (Han et al., 2011). The inner domain (Fig. 1) has 94 × 90 grid cells and a 16 km resolution on a rotated polar stereographic map projection centered at (116° E, 40 °N). This domain includes all major regions in NCP, namely, Beijing, Tianjin, Hebei, Shandong, and Shanxi. Fifteen vertical levels, nearly half of which were concentrated in the lowest 2 km, were used to improve the simulation of the atmospheric boundary layer. The positions of the measurement stations applied for model evaluation are marked on Fig. 1.

### 3 Model evaluation

In this section, the model simulations are compared with the observations. The meteorological driver is an important factor in aerosol and visibility simulation. Wind vector, temperature, and relative humidity are inherently related to aerosol transport, scavenging, and water uptake effect. Thus, the monitoring data from the surface stations of the Chinese National Meteorological Center (CNMC; <http://cdc.cma.gov.cn/home.do>) were collected to evaluate the performance of the meteorological field simulation. CNMC has 726 measurement stations that are evenly distributed throughout mainland China and has been providing long-term surface observations of several meteorological variables since 1 January 1951 (Feng et al., 2004).

The comparative results of the daily average temperature, relative humidity, wind speed, and maximum wind direction at eight stations in February and July are shown in Figs. 2 to 5, respectively. The modeled temperature, relative humidity, and wind speed were in good agreement with the observations at nearly all stations. A persistent underestimation of wind speed by the models was found at the Wutaishan and Taishan sites. The modeled wind speed presented in Fig. 4 was obtained by converting the output values of the first layer (90 m to 200 m) to near-surface wind (~ 10 m) according to Monin–Obukhov similarity theory (Ding et al., 2001). These two sites are

## Modeling analysis of the seasonal characteristics of haze formation

X. Han et al.

Title Page

Abstract

Introduction

Conclusions

References

Tables

Figures



Back

Close

Full Screen / Esc

Printer-friendly Version

Interactive Discussion



located on the mountainside at elevations of 2208 and 1533 m, respectively, thus, the underestimation may be attributed to the different elevations between the simulation and the observation. As shown in Fig. 5, the modeled wind directions did not coincide well with the observed data. A direct comparison is difficult to achieve because of the difference in time resolutions between the site measurements (10 min, average) and the model output (1 h). Nevertheless, the variation trends of the modeled and observed wind directions are similar at most sites, as shown in Fig. 5.

The modeled hourly  $\text{NO}_2$ ,  $\text{O}_3$ ,  $\text{PM}_{2.5}$ , and visibility in February and July were also compared with the observed data provided by the Chinese Research Academy of Environmental Sciences (CRAES); CRAES observes the real-time mass burden of air pollutants in Beijing (Gao et al., 2012). The comparative results are shown in Figs. 6 and 7. The model efficiently captured the daily variation of the pollutant gases and the high mass burden of  $\text{PM}_{2.5}$  in these two months; however, an overestimation of  $\text{PM}_{2.5}$  can be found in the middle of July, as shown in Fig. 6. The modeled visibility also agrees well with the observations, particularly for visibility lower than 10 km, suggesting that the model can provide reasonable simulation during haze occurrence. Meanwhile, continuous haze can be found in the modeled and observed results in the middle of July, as shown in Fig. 7. This phenomenon indicates that although the model overestimated the mass burden of  $\text{PM}_{2.5}$ , the visibility simulation during this period remains reliable.

The modeled daily average mass concentrations of major aerosol components were compared with the observed data from the CRAES measurements, as shown in Fig. 8. The observed data lacked information for the first half of February and a number of days in July because of instrument failure. Although the magnitudes of the mass concentrations between the simulation and the observation do not exactly agree with each other, the modeled results could broadly reproduce the peaks of the observed data on 20 February–23 February and 20–23 July; the modeled results could also follow the seasonal variation features. For instance, the modeled and observed carbonaceous aerosols were both high in February and low in July. The model demonstrated obvious systematic underestimation of organic carbon in these two months, as shown in Fig. 8.

Numerous studies have reported that such phenomenon is a common issue in regional chemistry and transport models (Heald et al., 2005; Koch et al., 2007). The simulation error is primarily due to the uncertainties in the estimation of VOCs and primary organic aerosol emissions and the formation mechanism of secondary organic aerosol (Kroll et al., 2006; Henze and Seinfeld, 2006; Yu et al., 2007). However, this discrepancy should not significantly affect the accuracy of the visibility simulation. Therefore, these evaluations suggest that the modeling system can reasonably simulate the meteorological field, the mass burdens of major aerosol components, and the surface visibility in February and July 2011.

## 4 Results and discussions

### 4.1 Distribution features of aerosol concentration and visibility

As shown in Figs. 6–8, two typical heavy air pollution episodes occurred over NCP on 20–23 February and 20 July–23 July. These two periods were selected to investigate the distribution features of pollutants and visibility over NCP during occurrences of heavy pollution in different seasons. Figure 9 presents the horizontal distributions of daily average mass concentration of  $\text{PM}_{2.5}$  and surface wind field over NCP on 20 February–23 February and 20–23 July. The heavy mass burden of  $\text{PM}_{2.5}$  (over  $120 \mu\text{g m}^{-3}$ ) was mainly concentrated in four urban areas, namely, Beijing (capital of China, municipality), Tianjin (municipality), Shijiazhuang (capital city of Hebei Province), and Jinan (capital city of Shandong Province), and their surrounding regions. The mass concentration of  $\text{PM}_{2.5}$  in February, which reached 200–300  $\mu\text{g m}^{-3}$  in the four urban areas and even exceeded 300  $\mu\text{g m}^{-3}$  in downtown Beijing, was obviously higher than that in July. The mass concentration of  $\text{PM}_{2.5}$  in July ranged of 75–200  $\mu\text{g m}^{-3}$  in the four urban areas and was rarely over 200  $\mu\text{g m}^{-3}$  over the entire NCP. The high mass burden of  $\text{PM}_{2.5}$  in Beijing generally appeared when NCP was dominated by the south wind field, which could have brought pollutants from the polluted

regions in the south. The heavy  $\text{PM}_{2.5}$  mass burden was also possibly transported to Northeast China and Bohai Sea by the strong south wind from 22–23 February and on 23 July, respectively, thereby increasing the mass concentration of  $\text{PM}_{2.5}$  by  $45 \mu\text{g m}^{-3}$  to  $125 \mu\text{g m}^{-3}$  in these two regions, as shown in Fig. 9.

Figure 9 also presents the horizontal distributions of daily average visibility and surface relative humidity over NCP. The data shows that haze cloud could spread throughout NCP during each pollution episode. The visibility in most parts of Hebei and Shandong was generally less than 8 km, which could decrease to 3–5 km in the four urban areas in February and July. The distribution patterns of visibility broadly followed those of the  $\text{PM}_{2.5}$  mass burden, and deteriorated visibility mainly appeared in the regions where the heavy  $\text{PM}_{2.5}$  mass burden is concentrated. The visibility generally decreased to 3–5 km when the mass concentration of  $\text{PM}_{2.5}$  exceeded  $200 \mu\text{g m}^{-3}$  in February. However, similar values of visibility also appeared in July when the mass concentration of  $\text{PM}_{2.5}$  was merely in the range of  $120\text{--}200 \mu\text{g m}^{-3}$ . Such phenomenon was demonstrated on 23 July when the visibility over the entire Bohai Sea generally ranged of 3–5 km and the mass concentration of  $\text{PM}_{2.5}$  was maintained between 120 and  $200 \mu\text{g m}^{-3}$ . These differences may be due to the strong extinction of soluble particles caused by the high relative humidity (exceeding 70 %) in July, as shown in Fig. 9. This feature is discussed in detail below.

## 4.2 Time series of meteorological, aerosol, and visibility characteristics in Beijing

Figure 10a–f present the time series of regional average surface wind speed, and relative humidity, visibility, as well as the mass concentrations of  $\text{PM}_{2.5}$ , sulfate, nitrate, ammonium, BC, and OC in Beijing in February and July 2011. The averages of these variables during the haze days in February and July are shown in Table 2. The mass burden of  $\text{PM}_{2.5}$  is the most important influencing factor of visibility change because it is generally inversely correlated with the variation of visibility. The mass concentrations of

### Modeling analysis of the seasonal characteristics of haze formation

X. Han et al.

Title Page

Abstract

Introduction

Conclusions

References

Tables

Figures

⏪

⏩

◀

▶

Back

Close

Full Screen / Esc

Printer-friendly Version

Interactive Discussion



increase. The detailed information during these two periods is shown in Fig. 11, which also shows the regional average vertical distribution of virtual potential temperature in Beijing. The mass concentration of  $\text{PM}_{2.5}$  decreased by over  $150 \mu\text{g m}^{-3}$  within 12 h when the wind speed decreased (from approximately  $6 \text{ m s}^{-1}$  to  $2 \text{ m s}^{-1}$ ) on 17 February or was approximately  $4 \text{ m s}^{-1}$  on 7 July. This phenomenon could be attributed to the vertical distribution of virtual potential temperature. A significant temperature inversion existed from 15–18 February, except during the daytime of 17 February, indicating that the vertical convection is beneficial to pollutant scavenging. A similar condition was observed appeared on 7 July. This feature clearly indicates that atmospheric vertical stability plays an important role in pollutant scavenging in Beijing. Moreover, the mass concentration of  $\text{PM}_{2.5}$  could obviously increase when temperature inversion and decrease in wind speed occurs simultaneously, as shown in Fig. 11.

### 4.3 Contribution of major aerosol components to extinction and sensitivity test

Figure 10g and h presents the time series of the regional average contribution ratios of sulfate, nitrate, ammonium, BC, OC, and other components (dust, sea salt, and unspecified anthropogenic mass) to the total surface extinction in Beijing in February and July. The monthly mean of these contribution ratios are shown in Table 3. The contribution ratios were calculated by subtracting the extinction coefficient with and without each aerosol component. Nitrate, sulfate, and ammonium, which are inorganic salts, significantly contributed to the surface extinction in Beijing, which was  $\sim 70\%$  in February and over  $80\%$  in July. Carbonaceous aerosol provided nearly  $20\%$  and  $5\%$  contribution in February and July, respectively, whereas other aerosol components provided  $\sim 10\%$  contribution. These values ratios generally followed the magnitude of their mass concentrations. Except for the diurnal variation of nitrate in July, the contribution ratios of each aerosol component did not significantly change when the mass concentration of  $\text{PM}_{2.5}$  exceeded  $\sim 50 \mu\text{g m}^{-3}$ . By contrast, when the mass concentration of  $\text{PM}_{2.5}$  decreased to less than  $50 \mu\text{g m}^{-3}$ , the contribution ratios of carbonaceous aerosol and

## Modeling analysis of the seasonal characteristics of haze formation

X. Han et al.

Title Page

Abstract

Introduction

Conclusions

References

Tables

Figures

◀

▶

◀

▶

Back

Close

Full Screen / Esc

Printer-friendly Version

Interactive Discussion

other components obviously increased. A higher mass concentration of PM<sub>2.5</sub> corresponds to higher contribution ratios of the three inorganic salts. This feature confirms that nitrate, sulfate, and ammonium are the major aerosol components that influence the haze formation in Beijing.

5 Considering that the PM<sub>2.5</sub> mass burden is an important influencing factor of the visibility variation, a sensitivity test was conducted to evaluate the mass concentration threshold of PM<sub>2.5</sub> to cause haze occurrence in Beijing. First, the mass ratio of each aerosol component to the total mass burden of all aerosol particles was calculated from the results of the model simulation at every grid point. Then, the sensitivity run was conducted by using several possible values of the total aerosol burden and following the same ratio of each aerosol component at the same grid points to identify the mass concentration threshold of PM<sub>2.5</sub> when the visibility decreased to 10 km under different relative humidity. The values of relative humidity were chosen as follows: 70 %, 75 %, 80 %, 85 %, 88 %, 89 %, and 90 %. Lower values of relative humidity were disregarded because the water uptake of soluble particles is insignificant when the relative humidity is less than 70 %. Figure 12a and b presents the time series of the regional average mass concentration threshold of PM<sub>2.5</sub> under different values of relative humidity from the sensitivity test in February and July in Beijing. The monthly means of the mass concentration threshold are shown in Table 4. The threshold changed significantly with the variation in relative humidity, and its declining trend increased with increasing relative humidity. The range of mass concentration threshold reached 30  $\mu\text{g m}^{-3}$  when the relative humidity changed from 70 % to 90 %. Conversely, the threshold generally maintained a small value range (< 5  $\mu\text{g m}^{-3}$ ) when the relative humidity was fixed. However, the mass concentration threshold on 29 July could increase by approximately 10  $\mu\text{g m}^{-3}$  under the same relative humidity, as shown in Fig. 12b. Further analysis showed that this phenomenon is related to the variation in aerosol size distribution. Figure 12c–h presents the time series of the regional average mass ratios of the three particle modes to the total aerosol burden. The mass ratio of the Aitken mode dramatically increased (~ 10 %) on 29 July. Therefore, the primary reason for the threshold fluctuation is that

## Modeling analysis of the seasonal characteristics of haze formation

X. Han et al.

Title Page

Abstract

Introduction

Conclusions

References

Tables

Figures

⏪

⏩

◀

▶

Back

Close

Full Screen / Esc

Printer-friendly Version

Interactive Discussion



## Modeling analysis of the seasonal characteristics of haze formation

X. Han et al.

Title Page

Abstract

Introduction

Conclusions

References

Tables

Figures

⏪

⏩

◀

▶

Back

Close

Full Screen / Esc

Printer-friendly Version

Interactive Discussion



the extinction efficiency of the Aitken mode particles was weaker than that of the accumulation mode particles. This feature clearly indicates that aerosol size distribution is an important influencing factor of haze occurrence in Beijing. The mass ratios of the coarse and accumulation modes changed by over 15 % during 6–10 July; however, the fluctuation of mass concentration threshold was much weaker than that on 29 July. This feature implies that the threshold can be easily influenced by particles of smaller size.

## 5 Conclusions

In this study, the air quality modeling system RAMS-CMAQ coupled with an aerosol optical property scheme was used to simulate the meteorological field, the mass concentration of aerosols, and the surface visibility over NCP in 2011. The modeling system provided reliable simulation results. The distribution patterns and time series of related meteorological factors and aerosol characteristic in February and July 2011 were analyzed to elucidate the seasonal variation features of the haze formation mechanism in Beijing and its surrounding regions. In addition, a sensitivity test was conducted to investigate the mass concentration threshold of haze occurrence in Beijing under distinct conditions. The results are summarized as follows:

1. The simulation results showed that the high mass burden of  $PM_{2.5}$  over NCP was mainly concentrated in the urban areas of Beijing, Tianjin, Shijiazhuang, Jinan, and their surrounding regions. The daily average mass concentration of  $PM_{2.5}$  over these regions was generally over  $120 \mu\text{g m}^{-3}$  during the pollution episodes in February and July. The worst air quality over NCP was found in Beijing because of the heavy daily average mass burden of  $PM_{2.5}$ , which exceeded  $300 \mu\text{g m}^{-3}$  in February. The south wind that carries pollutants from the southern regions is an important source of the heavy aerosol loading in Beijing. In addition to the horizontal diffusion, the vertical convection also plays an important role in the pollutant scavenging in Beijing.





## Modeling analysis of the seasonal characteristics of haze formation

X. Han et al.

Title Page

Abstract

Introduction

Conclusions

References

Tables

Figures

⏪

⏩

◀

▶

Back

Close

Full Screen / Esc

Printer-friendly Version

Interactive Discussion

Ding, F., Pal Arya, S., and Lin, Y.: Large-eddy simulations of the atmospheric boundary layer using a new subgrid-scale model-I I. Weakly and moderately stable cases, *Environ. Fluid Mech.*, 1, 49–69, 2001.

Eder, B. and Yu, S. C.: An evaluation of model performance of EPA models-3/CMAQ, *Atmos. Environ.*, 40, 4811–4824, 2006.

Eder, B., Kang, D., Mathur, R., Pleim, J., Yu, S. C., Otte, T., and Pouliot., G.: A performance evaluation of the national air quality forecast capability for the summer of 2007, *Atmos. Environ.*, 43, 2312–2320, 2009.

Feng, S., Hu, Q., and Qian, W.: Quality control of daily meteorological data in China, 1951–2000: a new dataset, *Int. J. Climatol.*, 24, 853–870, 2012.

Gao, J., Zhang, Y., Wang, S., Chi, F., and Chen, Y.: Study on the Characteristics and Formation of a Multi-Day Haze in October 2011 in Beijing, *Res. Environ. Sci.*, 25, 1201–1207, 2012 (in Chinese).

Ghan, S. and Zaveri, R.: Parameterization of optical properties for hydrated internally mixed aerosol, *J. Geophys. Res.*, 112, D10201, doi:10.1029/2006JD007927, 2007.

Gong, S. L.: A parameterization of sea-salt aerosol source function for sub- and super-micron particles, *Global Biogeochem. Cy.*, 17, 1097, doi:10.1029/2003GB002079, 2003.

Han, X., Zhang, M., Han, Z., Xin, J., and Liu, X.: Simulation of aerosol direct radiative forcing with RAMS-CMAQ in East Asia, *Atmos. Environ.*, 45, 6576–6592, 2011.

Han, X., Zhang, M., Tao, J., Wang, L., Gao, J., Wang, S., Chai, F.: Modeling aerosol impacts on atmospheric visibility in Beijing with RAMS-CMAQ, *Atmos. Environ.*, 72, 177–191, 2013.

Han, Z., Ueda, H., Matsuda, K., Zhang, R., Arao, K., Kanai, Y., and Hasome, H.: Model study on particle size segregation and deposition during Asian dust events in March 2002, *J. Geophys. Res.*, 109, D19205, doi:10.1029/2004JD004920, 2004.

Hao, J. and Wang, L.: Improving Urban Air Quality in China: Beijing Case Study, *Air Waste Manage. Assoc.*, 62, 1298–1305, 2012.

Heald, C. L., Jacob, D. J., Park, R. J., Russell, L. M., Huebert, B. J., Seinfeld, J. H., Liao, H., and Weber, R. J.: A large organic aerosol source in the free troposphere missing from current models, *Geophys. Res. Lett.*, 32, L18809, doi:10.1029/2005GL023831, 2005.

Henze, D. K. and Seinfeld, J. H.: Global secondary organic aerosol from isoprene oxidation, *Geophys. Res. Lett.*, 33, L09812, doi:10.1029/2006GL025976, 2006.

**Modeling analysis of  
the seasonal  
characteristics of  
haze formation**

X. Han et al.

Title Page

Abstract

Introduction

Conclusions

References

Tables

Figures

⏪

⏩

◀

▶

Back

Close

Full Screen / Esc

Printer-friendly Version

Interactive Discussion

- Koch, D., Bond, T. C., Streets, D., Unger, N., van der Werf, G. R.: Global impact of aerosols from particular source regions and sectors, *J. Geophys. Res.*, 112, D02205, doi:10.1029/2005JD007024, 2007.
- 5 Kroll, J. H., Ng, N. L., Murphy, S. M., Flagan, R. C., and Seinfeld, J. H.: Secondary organic aerosol formation from isoprene photooxidation, *Environ. Sci. Technol.*, 40, 1869–1877, 2006.
- Li, W. J., Shao, L. Y., and Buseck, P. R.: Haze types in Beijing and the influence of agricultural biomass burning, *Atmos. Chem. Phys.*, 10, 8119–8130, doi:10.5194/acp-10-8119-2010, 2010.
- 10 Li, Z., Gu, X., Wang, L., Li, D., Xie, Y., Li, K., Dubovik, O., Schuster, G., Goloub, P., Zhang, Y., Li, L., Ma, Y., and Xu, H.: Aerosol physical and chemical properties retrieved from ground-based remote sensing measurements during heavy haze days in Beijing winter, *Atmos. Chem. Phys.*, 13, 10171–10183, doi:10.5194/acp-13-10171-2013, 2013.
- 15 Liu, X. G., Li, J., Qu, Y., Han, T., Hou, L., Gu, J., Chen, C., Yang, Y., Liu, X., Yang, T., Zhang, Y., Tian, H., and Hu, M.: Formation and evolution mechanism of regional haze: a case study in the megacity Beijing, China, *Atmos. Chem. Phys.*, 13, 4501–4514, doi:10.5194/acp-13-4501-2013, 2013.
- Lu, Z., Streets, D. G., Zhang, Q., Wang, S., Carmichael, G. R., Cheng, Y. F., Wei, C., Chin, M., Diehl, T., and Tan, Q.: Sulfur dioxide emissions in China and sulfur trends in East Asia since 2000, *Atmos. Chem. Phys.*, 10, 6311–6331, doi:10.5194/acp-10-6311-2010, 2010.
- 20 Lu, Z., Zhang, Q., and Streets, D. G.: Sulfur dioxide and primary carbonaceous aerosol emissions in China and India, 1996–2010, *Atmos. Chem. Phys.*, 11, 9839–9864, doi:10.5194/acp-11-9839-2011, 2011.
- Ma, J., Xu, X., Zhao, C., and Yan, P.: A review of atmospheric chemistry research in China: photochemical smog, haze pollution, and gas-aerosol interactions, *Adv. Atmos. Sci.*, 29, 1006–1026, 2010.
- 25 Mathur, R., Yu, S. C., Kang, D., and Schere, K. L.: Assessment of the winter-time performance of developmental particulate matter forecasts with the Eta-CMAQ modeling system, *J. Geophys. Res.*, 113, D02303, doi:10.1029/2007JD008580, 2008.
- 30 Nenes, A., Pandis, S., and Pilinis, C.: Continued development and testing of a new thermodynamic aerosol module for urban and regional air quality models, *Atmos. Environ.*, 33, 1553–1560, 1999.

**Modeling analysis of  
the seasonal  
characteristics of  
haze formation**

X. Han et al.

Title Page

Abstract

Introduction

Conclusions

References

Tables

Figures

◀

▶

◀

▶

Back

Close

Full Screen / Esc

Printer-friendly Version

Interactive Discussion

- Pruppacher, H. and Klett, J.: *Microphysics of Clouds and Precipitation*, Springer, New York, 954 pp., 1997.
- Quan, J., Zhang, Q., He, H., Liu, J., Huang, M., and Jin, H.: Analysis of the formation of fog and haze in North China Plain (NCP), *Atmos. Chem. Phys.*, 11, 8205–8214, doi:10.5194/acp-11-8205-2011, 2011.
- 5 Randerson, J. T., van der Werf, G. R., Giglio, L., Collatz, G. J., and Kasibhatla, P. S.: Global Fire Emissions Database, Version 2 (GFEDv2.1), Data set available at: <http://daac.ornl.gov/>, Oak Ridge National Laboratory Distributed Active Archive Center, Oak Ridge, Tennessee, USA, doi:10.3334/ORNLDAAAC/849, 2007.
- 10 Sarwar, G., Luecken, D., Yarwood, G., Whitten, G., and Carter, W.: Impact of an updated carbon bond mechanism on predictions from the CMAQ modeling system: preliminary assessment, *J. Appl. Meteorol. Clim.*, 47, 3–14, 2008.
- Seinfeld, J. and Pandis, S.: *Atmosphere Chemistry and Physics*, Wiley, New York, USA, 1998.
- Sun, Y., Zhuang, G., Tang, A., Wang, Y., and An, Z.: Chemical characteristics of PM<sub>2.5</sub> and PM<sub>10</sub> in Haze-Fog episodes in Beijing, *Environ. Sci. Technol.*, 40, 3148–3155, 2006.
- 15 Tao, M., Chen, L., Su, L., and Tao, J.: Satellite observation of regional haze pollution over the North China Plain, *J. Geophys. Res.*, 117, D12203, doi:10.1029/2012JD017915, 2012.
- Wang, X., Sun, M., Yang, T., and Wang, Z.: Interdecadal change in frequency of dust-haze episodes in North China Plain, *Clim. Environ. Res.*, 18, 165–170, 2013 (in Chinese).
- 20 Wang, Y., Zhuang, G., Sun, Y., An, Z.: The variation of characteristics and formation mechanisms of aerosols in dust, haze, and clear days in Beijing, *Atmos. Environ.*, 40, 6579–6591, 2006.
- Wu, D., Bi, X., Deng, X., Li, F., Tan, H.: Effect of atmospheric haze on the deterioration of visibility over the Pearl River Delta, *Acta Geogr. Sin.*, 21, 215–223, 2007 (in Chinese).
- 25 Yu, S. C., Bhawe, P. V., Dennis, R. L., and Mathur, R.: Seasonal and regional variations of primary and secondary organic aerosols over the continental United States: semi-empirical estimates and model evaluation, *Environ. Sci. Technol.*, 41, 4690–4697, 2007.
- Yu, S., Mathur, R., Pleim, J., Wong, D., Gilliam, R., Alapaty, K., Zhao, C., and Liu, X.: Aerosol indirect effect on the grid-scale clouds in the two-way coupled WRF-CMAQ: model description, development, evaluation and regional analysis, *Atmos. Chem. Phys. Discuss.*, 13, 25649–25739, doi:10.5194/acpd-13-25649-2013, 2013.
- 30 Yu, X., Zhu, B., Yin, Y., Yang, J., Li, Y., and Bu, X.: A comparative analysis of aerosol properties in dust and haze-fog days in a Chinese urban region, *Atmos. Res.*, 99, 241–247, 2011.

## Modeling analysis of the seasonal characteristics of haze formation

X. Han et al.

Title Page

Abstract

Introduction

Conclusions

References

Tables

Figures

⏪

⏩

◀

▶

Back

Close

Full Screen / Esc

Printer-friendly Version

Interactive Discussion

- Zhang, A., Qi, Q., Jiang, L., Zhou, F., and Wang, J.: Population exposure to PM<sub>2.5</sub> in the urban area of Beijing, PloS one, 8, e63486, doi:10.1371/journal.pone.0063486, 2013.
- Zhang, J., Miao, H., Ouyang, Z., and Wang, X.: Ambient air quality trends and driving factor analysis since 1980's in Beijing, Acta Sci. Circumstantiae, 26, 1886–1892, 2006 (in Chinese).
- Zhang, J. P., Zhu, T., Zhang, Q. H., Li, C. C., Shu, H. L., Ying, Y., Dai, Z. P., Wang, X., Liu, X. Y., Liang, A. M., Shen, H. X., and Yi, B. Q.: The impact of circulation patterns on regional transport pathways and air quality over Beijing and its surroundings, Atmos. Chem. Phys., 12, 5031–5053, doi:10.5194/acp-12-5031-2012, 2012.
- Zhang, M., Xu, Y., Zhang, R., and Han, Z.: Emission and concentration distribution of black carbon aerosol in East Asia during springtime, Chin. J. Geophys., 48, 55–61, 2005.
- Zhang, M., Uno, I., Zhang, R., Han, Z., Wang, Z., and Pu, Y.: Evaluation of the Models-3 Community Multi-scale Air Quality (CMAQ) modeling system with observations obtained during the TRACE-P experiment: comparison of ozone and its related species, Atmos. Environ., 40, 4874–4882, 2006.
- Zhang, M., Gao, L., Ge, C., and Y.: Simulation of nitrate aerosol concentrations over East Asia with the model system RAMS-CMAQ, Tellus B, 59, 372–380, 2007.
- Zhao, P., Zhang, X., Xu, X., and Zhao, X.: Long-term visibility trends and characteristics in the region of Beijing, Tianjin, and Hebei, China, Atmos. Res., 101, 711–718, 2011.
- Zhao, X. J., Zhao, P. S., Xu, J., Meng, W., Pu, W. W., Dong, F., He, D., and Shi, Q. F.: Analysis of a winter regional haze event and its formation mechanism in the North China Plain, Atmos. Chem. Phys., 13, 5685–5696, doi:10.5194/acp-13-5685-2013, 2013.

## Modeling analysis of the seasonal characteristics of haze formation

X. Han et al.

Title Page

Abstract

Introduction

Conclusions

References

Tables

Figures

⏪

⏩

◀

▶

Back

Close

Full Screen / Esc

Printer-friendly Version

Interactive Discussion



**Table 1.** Aerosol size distribution parameters in RAMS-CMAQ.

Mode	Aerosol components	$\sigma^a$	$r^b, \mu\text{m}$
Aitken	ASO <sub>4</sub> <sup>c</sup> , ANO <sub>3</sub> <sup>d</sup> , ANH <sub>4</sub> <sup>e</sup> , BC <sup>f</sup> , OC <sup>g</sup>	1.7	0.015
Accumulation	ASO <sub>4</sub> , ANO <sub>3</sub> , ANH <sub>4</sub> , BC, OC, Dust, Sea salt	2.0	0.150
Coarse dust	Dust	3.0	0.300
Coarse sea salt	Sea salt	3.5	0.300

<sup>a</sup>  $\sigma$  is geometric standard deviation.

<sup>b</sup>  $r$  is mode radius.

<sup>c</sup> ASO<sub>4</sub> represents sulfate aerosol.

<sup>d</sup> ANO<sub>3</sub> represents nitrate aerosol.

<sup>e</sup> ANH<sub>4</sub> represents ammonium aerosol.

<sup>f</sup> BC represents black carbon.

<sup>g</sup> OC represents organic carbon.

## Modeling analysis of the seasonal characteristics of haze formation

X. Han et al.

Title Page

Abstract

Introduction

Conclusions

References

Tables

Figures

◀

▶

◀

▶

Back

Close

Full Screen / Esc

Printer-friendly Version

Interactive Discussion

**Table 2.** The number of haze days in February and July in Beijing. Also shown are the regional and temporal average surface wind speed ( $\text{m s}^{-1}$ ), and visibility (km), relative humidity (%), as well as mass concentrations ( $\mu\text{g m}^{-3}$ ) of sulfate, nitrate, ammonium, BC, OC, and  $\text{PM}_{2.5}$  during the haze days in February and July, respectively, in Beijing.

variables		Feb	Jul
Number of haze days		7	13
Wind speed		3.13	3.41
Visibility		6.22	5.73
Relative humidity		55.80	74.32
Mass concentration	Sulfate	37.99	52.32
	Nitrate	54.78	48.37
	Ammonium	30.15	33.60
	BC	13.29	4.31
	OC	19.51	5.16
	$\text{PM}_{2.5}$	174.26	148.32

**Modeling analysis of the seasonal characteristics of haze formation**

X. Han et al.

[Title Page](#)[Abstract](#)[Introduction](#)[Conclusions](#)[References](#)[Tables](#)[Figures](#)[◀](#)[▶](#)[◀](#)[▶](#)[Back](#)[Close](#)[Full Screen / Esc](#)[Printer-friendly Version](#)[Interactive Discussion](#)

**Table 3.** Regional and monthly average extinction contribution ratios (%) of sulfate, nitrate, ammonium, BC, OC, and other aerosols (dust, sea salt, and unspecified anthropogenic mass) in February and July, respectively, in Beijing.

	Sulfate	Nitrate	Ammonium	BC	OC	Others
Feb	22.73	29.69	17.13	5.05	13.22	12.18
Jul	39.31	24.77	21.88	0.33	3.96	9.74

## Modeling analysis of the seasonal characteristics of haze formation

X. Han et al.

Title Page

Abstract

Introduction

Conclusions

References

Tables

Figures

◀

▶

◀

▶

Back

Close

Full Screen / Esc

Printer-friendly Version

Interactive Discussion

**Table 4.** Regional and monthly average mass concentration threshold of  $\text{PM}_{2.5}$  ( $\mu\text{g m}^{-3}$ ) under different relative humidity from the sensitivity test in Beijing.

	70%	75%	80%	85%	88%	89%	90%
Feb	82.08	78.01	72.34	64.54	58.27	55.87	53.22
Jul	83.08	78.64	72.46	64.01	57.35	54.82	52.10

**Modeling analysis of  
the seasonal  
characteristics of  
haze formation**

X. Han et al.

Title Page

Abstract

Introduction

Conclusions

References

Tables

Figures

◀

▶

◀

▶

Back

Close

Full Screen / Esc

Printer-friendly Version

Interactive Discussion

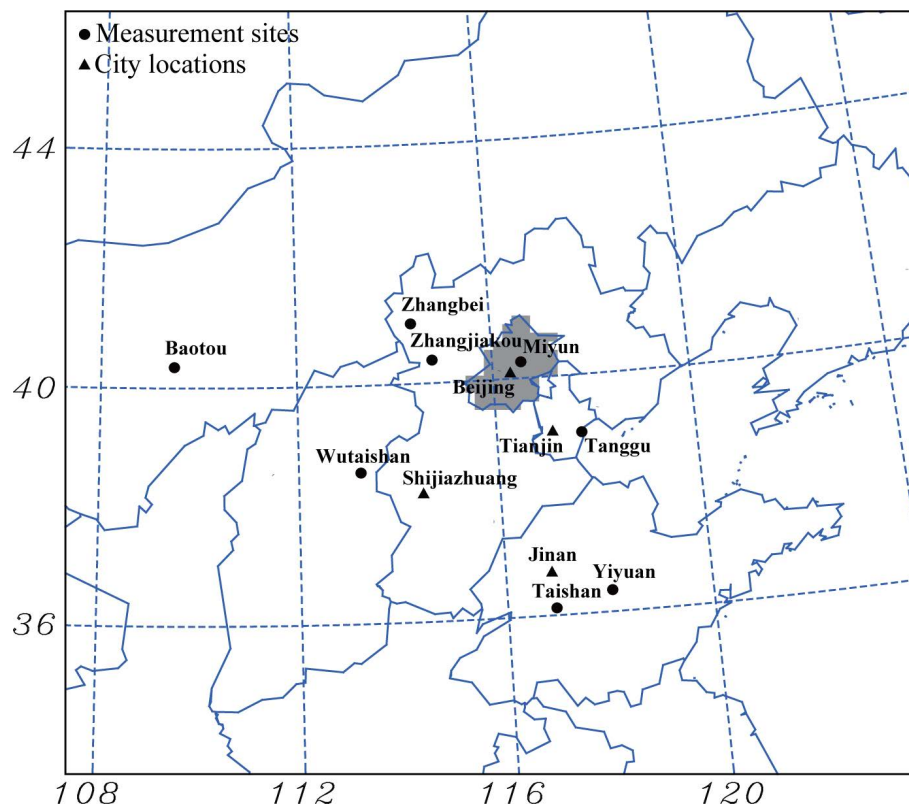


**Fig. 1.** Geographic location of API monitoring cities and CNMC measurement stations in the model domain. The gray area represents the district of Beijing megacity.

Modeling analysis of  
the seasonal  
characteristics of  
haze formation

X. Han et al.

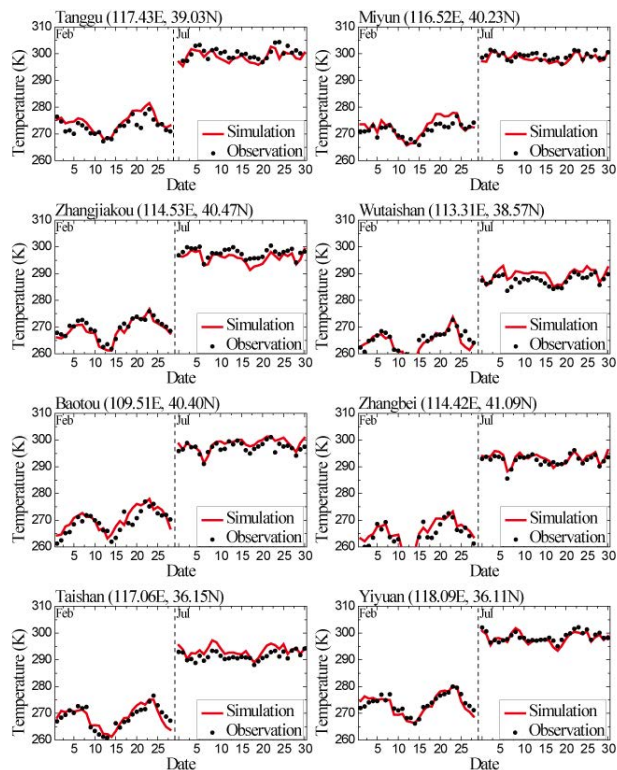


**Fig. 2.** Observed (circle) and modeled (solid line) daily average temperature (K) at 8 stations in February and July 2011.

## Modeling analysis of the seasonal characteristics of haze formation

X. Han et al.

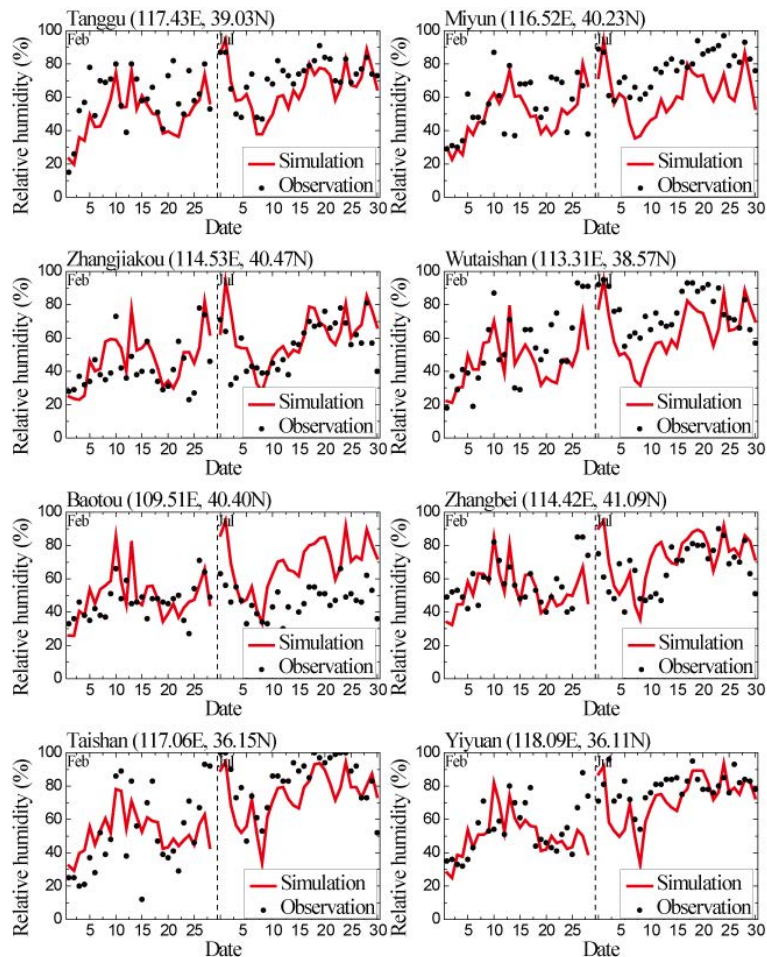


**Fig. 3.** Same as Fig. 2 but for relative humidity (%).

Title Page

Abstract

Introduction

Conclusions

References

Tables

Figures

◀

▶

◀

▶

Back

Close

Full Screen / Esc

Printer-friendly Version

Interactive Discussion

## Modeling analysis of the seasonal characteristics of haze formation

X. Han et al.

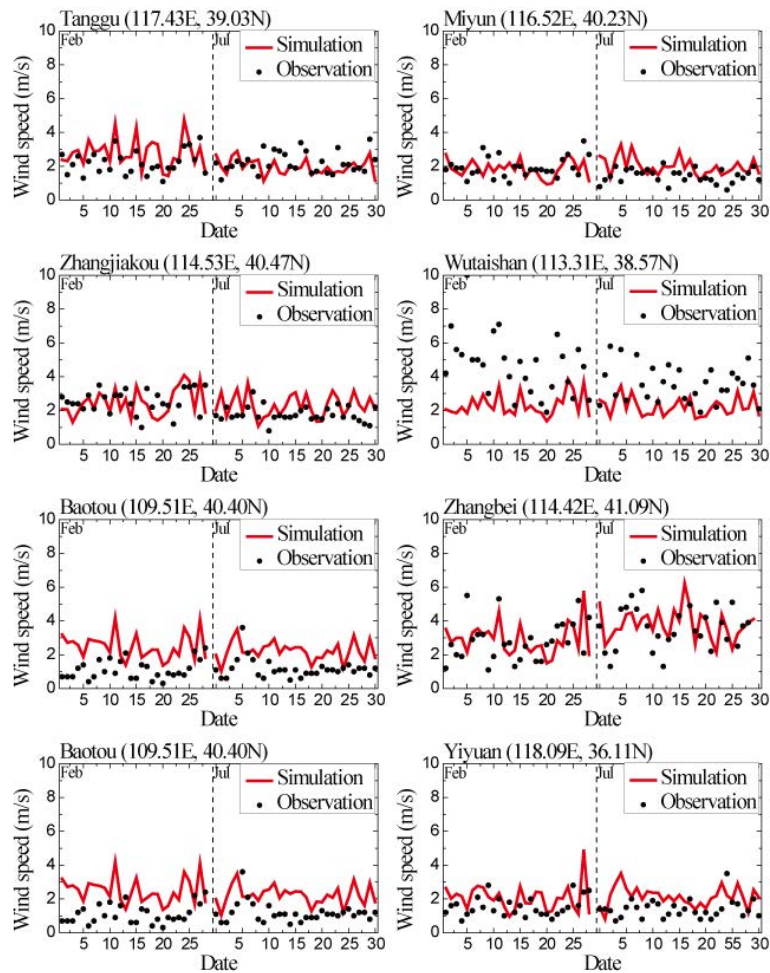
[Title Page](#)
[Abstract](#)
[Introduction](#)
[Conclusions](#)
[References](#)
[Tables](#)
[Figures](#)
[Back](#)
[Close](#)
[Full Screen / Esc](#)
[Printer-friendly Version](#)
[Interactive Discussion](#)


Fig. 4. Same as Fig. 2 but for wind speed ( $\text{ms}^{-1}$ ).

## Modeling analysis of the seasonal characteristics of haze formation

X. Han et al.

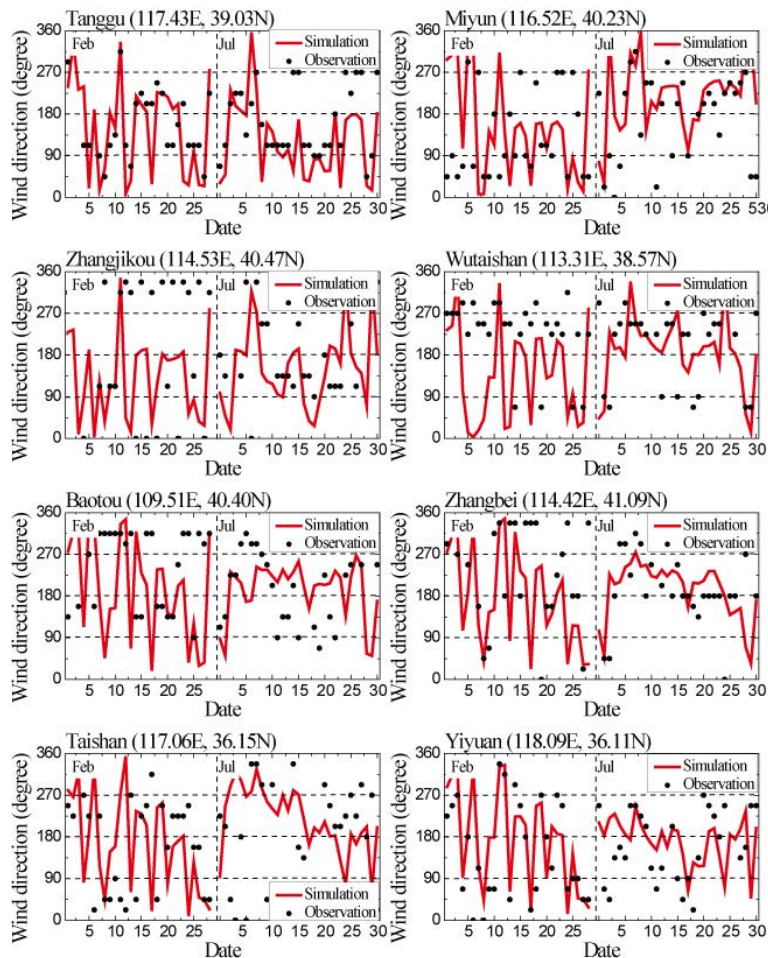


Fig. 5. Same as Fig. 2 but for wind direction (degree).

[Title Page](#)
[Abstract](#)
[Introduction](#)
[Conclusions](#)
[References](#)
[Tables](#)
[Figures](#)
[Back](#)
[Close](#)
[Full Screen / Esc](#)
[Printer-friendly Version](#)
[Interactive Discussion](#)

Modeling analysis of  
the seasonal  
characteristics of  
haze formation

X. Han et al.

Title Page

Abstract

Introduction

Conclusions

References

Tables

Figures

◀

▶

◀

▶

Back

Close

Full Screen / Esc

Printer-friendly Version

Interactive Discussion

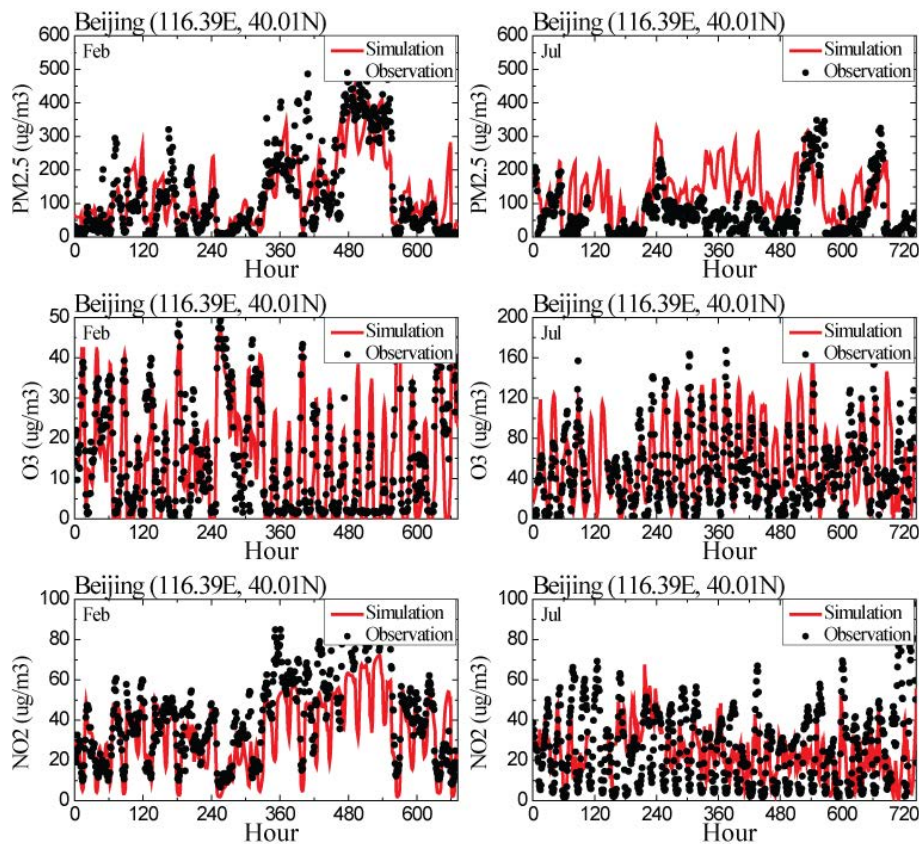


**Fig. 6.** Observed (circle) and modeled (line) hourly mass concentrations ( $\mu\text{g m}^{-3}$ ) of PM<sub>2.5</sub>, O<sub>3</sub>, and NO<sub>2</sub> in February and July 2011 at Beijing.



## Modeling analysis of the seasonal characteristics of haze formation

X. Han et al.

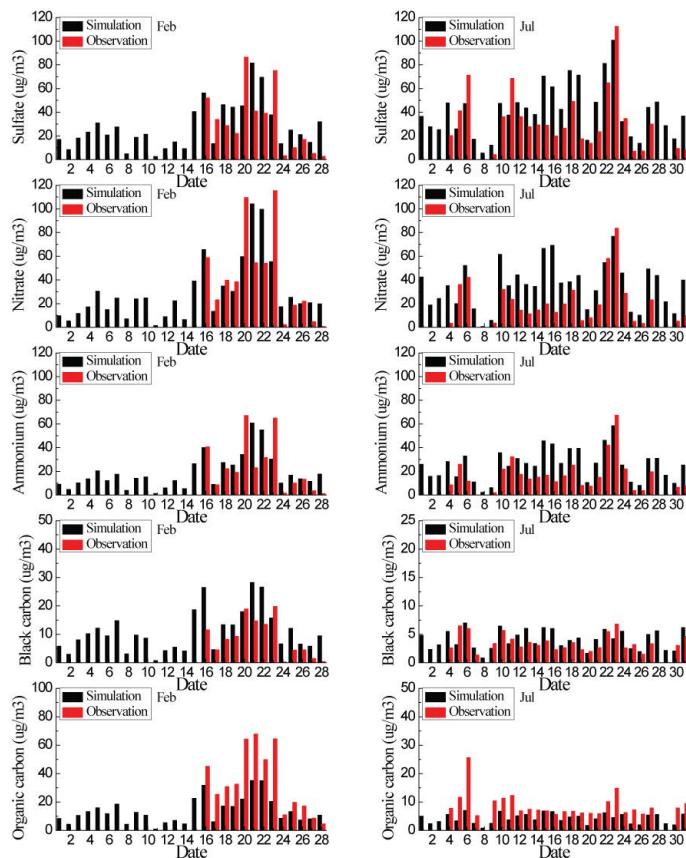


**Fig. 8.** Observed (circle) and modeled (line) daily average mass concentrations ( $\mu\text{g m}^{-3}$ ) of sulfate, nitrate, ammonium, black carbon, and organic carbon in February and July 2011 at Beijing.

[Title Page](#)
[Abstract](#)
[Introduction](#)
[Conclusions](#)
[References](#)
[Tables](#)
[Figures](#)
[⏪](#)
[⏩](#)
[⏴](#)
[⏵](#)
[Back](#)
[Close](#)
[Full Screen / Esc](#)
[Printer-friendly Version](#)
[Interactive Discussion](#)

## Modeling analysis of the seasonal characteristics of haze formation

X. Han et al.

Title Page

Abstract

Introduction

Conclusions

References

Tables

Figures

◀

▶

◀

▶

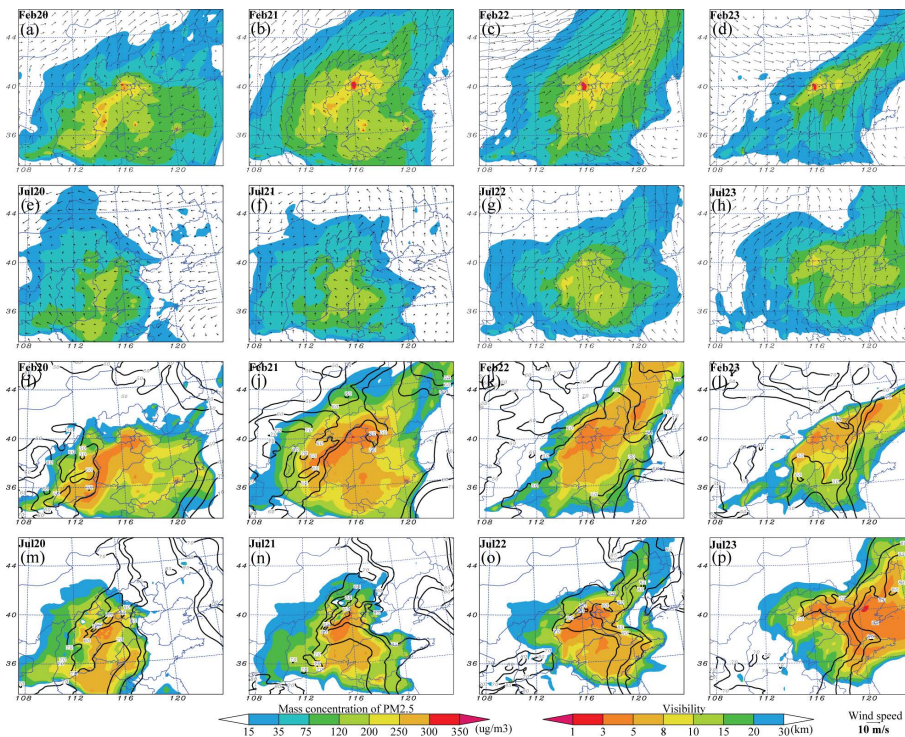
Back

Close

Full Screen / Esc

Printer-friendly Version

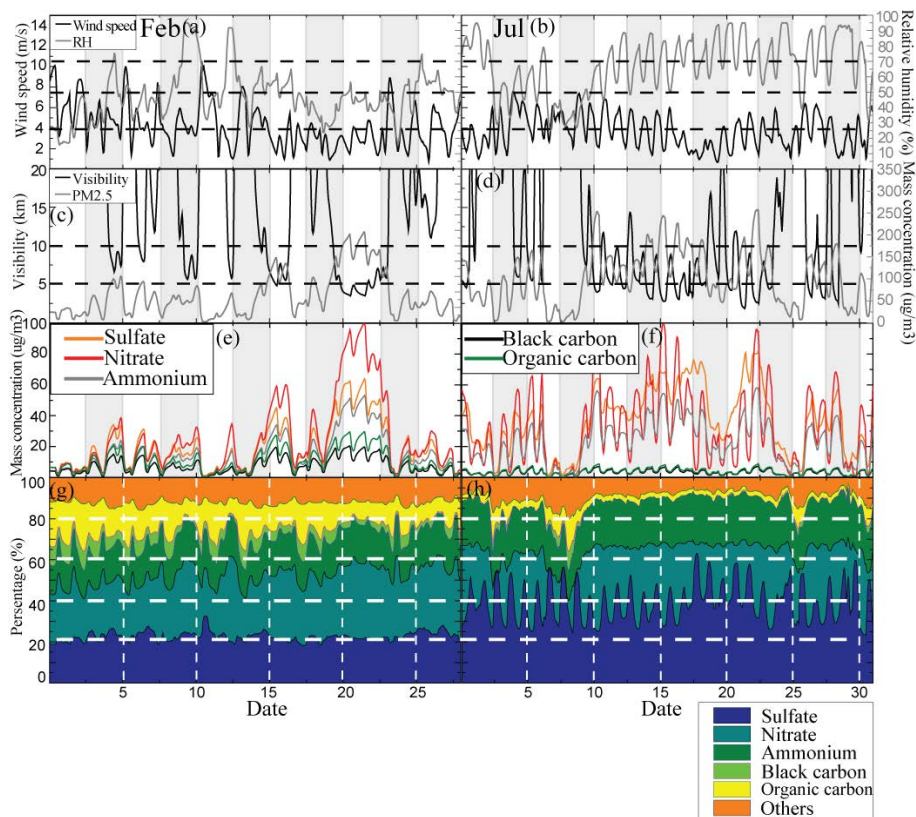
Interactive Discussion



**Fig. 9.** The horizontal distributions of daily average mass concentration of  $\text{PM}_{2.5}$  ( $\mu\text{g m}^{-3}$ ; **a–h**) and visibility (km; **i–p**) from 20 to 23 February and 20 to 23 July over NCP. Also shown is the wind field (arrows) and relative humidity (%; black contour lines).

## Modeling analysis of the seasonal characteristics of haze formation

X. Han et al.

[Title Page](#)
[Abstract](#)
[Introduction](#)
[Conclusions](#)
[References](#)
[Tables](#)
[Figures](#)
[Back](#)
[Close](#)
[Full Screen / Esc](#)
[Printer-friendly Version](#)
[Interactive Discussion](#)


**Fig. 10.** The time series of regional average surface wind speed ( $\text{m s}^{-1}$ ), and relative humidity (%), visibility (km), as well as  $\text{PM}_{2.5}$  mass concentrations ( $\mu\text{g m}^{-3}$ ) in February and July in Beijing (**a–d**). Also shown are the mass concentrations ( $\mu\text{g m}^{-3}$ ; **e, f**) and extinction contribution ratios (**g, h**) of sulfate, nitrate, ammonium, BC, OC, and other aerosols (dust, sea salt, and unspecified anthropogenic mass).

Modeling analysis of  
the seasonal  
characteristics of  
haze formation

X. Han et al.

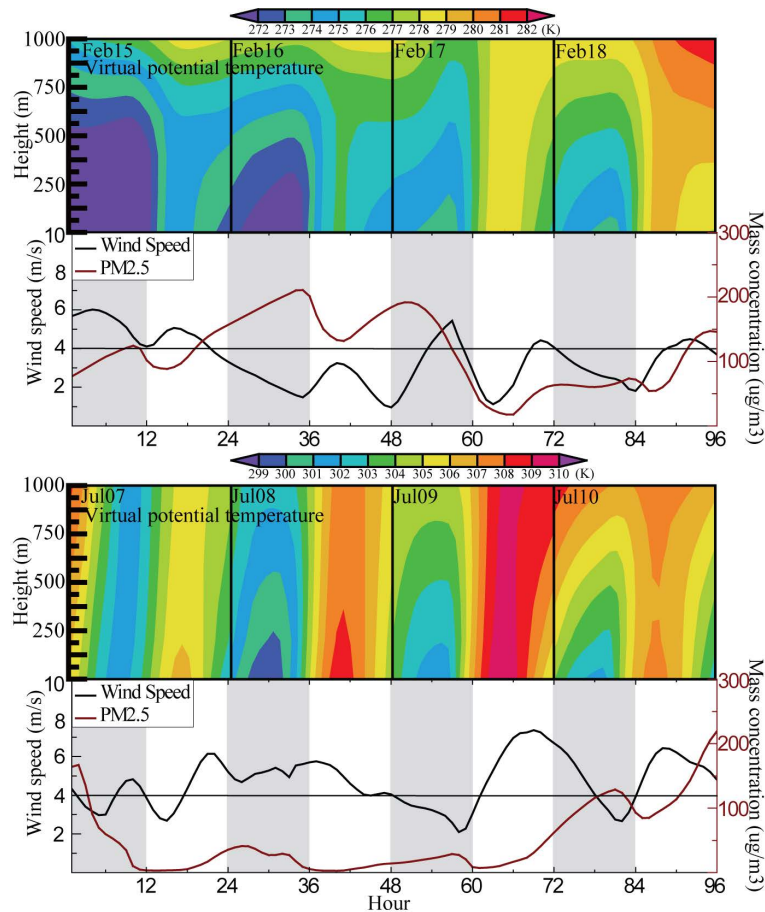


**Fig. 11.** The time series of regional average vertical distribution of virtual potential temperature (K) from 15 to 18 February and 7 to 10 July in Beijing. Also shown are the surface wind speed ( $\text{ms}^{-1}$ ) and mass concentration of  $\text{PM}_{2.5}$  ( $\mu\text{g m}^{-3}$ ).

## Modeling analysis of the seasonal characteristics of haze formation

X. Han et al.

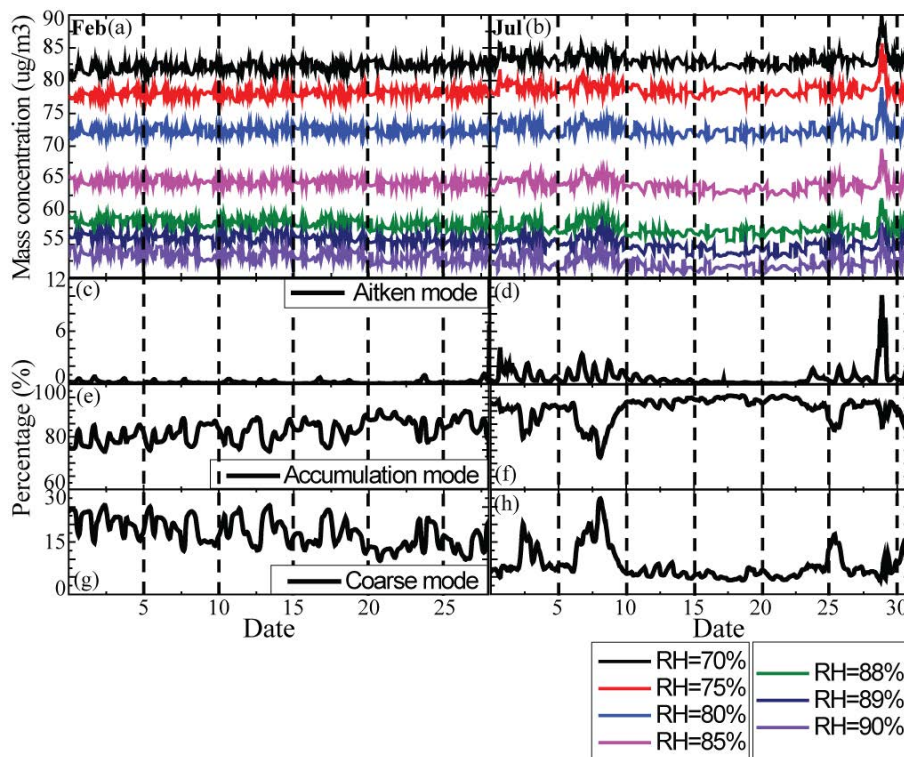


**Fig. 12.** The time series of regional average mass concentration threshold of  $PM_{2.5}$  under different relative humidity (%) from the sensitivity test in February and July in Beijing. Also shown are the mass ratio of Aitken mode, accumulation mode, and coarse mode.